Research Article | Vol. 25, No. 3 | 6 Feb 2017 | OPTICS EXPRESS 1789

Optics EXPRESS

Distributed photothermal spectroscopy in microstructured optical fibers: towards high-resolution mapping of gas presence over long distances

ANDRES GARCIA-RUIZ,[1,*] JUAN PASTOR-GRAELLS,[1] HUGO F. MARTINS,[2] KENNY HEY TOW,[3] LUC THÉVENAZ,[3] SONIA MARTIN-LOPEZ,[1] AND MIGUEL GONZALEZ-HERRAEZ[1]

[1]*Dpto. de Electrónica, University of Alcalá, 28805, Alcalá de Henares (Madrid), Spain*
[2]*FOCUS S. L., C/ Orellana, 1, 1º Izq., 28004, Madrid, Spain*
[3]*EPFL Swiss Federal Institute of Technology, Institute of Electrical Engineering, SCI STI LT, Station 11, CH-1015 Lausanne, Switzerland*
[*]*andres.garciaruiz@uah.es*

Abstract: Chemical sensing using optical fibers is often challenging, as it is generally difficult to achieve strong interaction between the guided light and the analyte at the wavelength of interest for performing the detection. Despite this difficulty, many schemes exist (and can be found in the literature) for point chemical fiber sensors. However, the challenge increases even further when it comes to performing fully distributed chemical sensing. In this case, the optical signal which interacts with the analyte is typically also the signal that has to travel to and from the interrogator: for a good sensitivity, the light should interact strongly with the analyte, leading inevitably to an increased loss and a reduced range. Few works in the literature actually provide demonstrations of truly distributed chemical sensing and, although there have been several attempts to realize these sensors (e.g. based on special fiber coatings), the vast majority of these attempts has failed to reach widespread use due to several reasons, among them: lack of sensitivity or selectivity, lack of range or resolution, cross sensitivity to temperature or strain, or need to work at specific wavelengths where fiber instrumentation becomes extremely expensive or unavailable. In this work we provide a preliminary demonstration of the possibility of achieving distributed detection of gas presence with spectroscopic selectivity, high spatial resolution, potential for long range measurements and feasibility of having most of the interrogator system working at conventional telecom wavelengths. For a full exploitation of this concept, new fibers (or more likely, fiber bundles) should be developed capable of guiding specific wavelengths in the IR (corresponding to gas absorption wavelengths) with good overlap with the analyte while also having a solid core with good transmission behavior at 1.55 μm, and good thermal coupling between the two guiding structures.

OCIS codes: (060.2370) Fiber optics sensors; (060.4005) Microstructured fibers; (060.5295) Photonic crystal fibers; (290.5870) Scattering, Rayleigh; (190.4870) Photothermal effects; (300.6430) Spectroscopy, photothermal; (280.1545) Chemical analysis.

References and links

1. M. Calcerrada, C. García-Ruiz, and M. González-Herráez, "Chemical and biochemical sensing applications of microstructured optical fiber-based systems," Laser Photon. Rev. **9**(6), 604–627 (2015).
2. R. L. Woodfin, *Trace Chemical Sensing of Explosives* (John Wiley & Sons, 2006).
3. R. Bharadwaj and S. Mukherji, "Gold nanoparticle coated U-bend fibre optic probe for localized surface plasmon resonance based detection of explosive vapours," Sensors Actuat B-Chem **192**, 804–811 (2014).
4. J. Kirsch, C. Siltanen, Q. Zhou, A. Revzin, and A. Simonian, "Biosensor technology: recent advances in threat agent detection and medicine," Chem. Soc. Rev. **42**, 8733–8768 (2013).
5. M. Marazuela and M. Moreno-Bondi, "Fiber-optic biosensors–an overview," Anal. Bioanal. Chem. **372**(5-6), 664–682 (2002).
6. G. A. Brown and A. Hartog, "Optical fiber sensors in upstream oil & gas," J. Petrol Technol. **54**(11), 63–65 (2002).

#279716 http://dx.doi.org/10.1364/OE.25.001789
Journal © 2017 Received 7 Nov 2016; revised 9 Jan 2017; accepted 10 Jan 2017; published 23 Jan 2017
Corrected: 24 January 2017

Optics EXPRESS

7. W. Cao and Y. Duan, "Optical fiber evanescent wave sensor for oxygen deficiency detection," Sensors Actuat B-Chem **119**(2), 363–369 (2006).
8. W. Jin, H. L. Ho, Y. C. Cao, J. Ju, and L. F. Qi, "Gas detection with micro- and nano-engineered optical fibers," Opt. Fiber Technol. **19**(6), 741–759 (2013).
9. W. Jin, Y. Cao, F. Yang, and H. L. Ho, "Ultra-sensitive all-fibre photothermal spectroscopy with large dynamic range," Nat. Commun. **6**, 6767 (2015).
10. J. B. Jensen, L. H. Pedersen, P. E. Hoiby, L. B. Nielsen, T. P. Hansen, J. R. Folkenberg, J. Riishede, D. Noordegraaf, K. Nielsen, A. Carlsen, and A. Bjarklev, "Photonic crystal fiber based evanescent-wave sensor for detection of biomolecules in aqueous solutions," Opt. Lett. **29**(17), 1974–1976 (2004).
11. S. M. Miller, S. C. Wofsy, A. M. Michalak, E. A. Kortc, A. E. Andrewsd, S. C. Biraude, E. J. Dlugokenckyd, J. Eluszkiewiczf, M. L. Fischerg, G. Janssens-Maenhouth, B. R. Milleri, J. B. Milleri, S. A. Montzkad, T. Nehrkornf, and C. Sweeneyi, "Anthropogenic emissions of methane in the United States," Proc. Natl. Acad. Sci. **110**(50), 20018–20022 (2013).
12. A. Boersma, M. Saalmink, T. Lucassen, S. Wiegersma, R. Jansen, R. Jansen, and L. Cheng, "Fiber Bragg distributed chemical sensor," in *Proceedings of IEEE Sensors* (IEEE, 2011).
13. Y. Koyamada, M. Imahama, K. Kubota, and K. Hogari, "Fiber-optic distributed strain and temperature sensing with very high measurand resolution over long range using coherent OTDR," J. Lightwave Technol. **27**(9), 1142–1146 (2009).
14. X. Bao and L. Chen, "Recent progress in distributed fiber optic sensors," Sensors **12**(7), 8601–8639 (2012).
15. M. Froggatt and J. Moore, "High-spatial-resolution distributed strain measurement in optical fiber with Rayleigh scatter," Appl. Opt. **37**(10), 1735–1740 (1998).
16. J. Tejedor, H. F. Martins, D. Piote, J. Macias-Guarasa, J. Pastor-Graells, S. Martin-Lopez, P. Corredera, F. De Smet, W. Postvoll, and M. Gonzalez-Herraez, "Towards Prevention of Pipeline Integrity Threats using a Smart Fiber Optic Surveillance System," J. Lightwave Technol. **PP.**(), 1 (2016).
17. H. F. Martins, D. Piote, J. Tejedor, J. Macias-Guarasa, J. Pastor-Graells, S. Martin-Lopez, P. Corredera, F. De Smet, W. Postvoll, C. H. Ahlen, and M. Gonzalez-Herraez, "Early detection of pipeline integrity threats using a smart fiber optic surveillance system: the PIT-STOP project," Proc. SPIE **9634**, 96347X (2015).
18. A. Dominguez-Lopez, Z. Yang, M. A. Soto, X. Angulo-Vinuesa, S. Martin-Lopez, L. Thévenaz, and M. Gonzalez-Herraez, "Novel scanning method for distortion-free BOTDA measurements," Opt. Express **24**(10), 10188–10204 (2016).
19. M. A. Soto, M. Taki, G. Bolognini, and F. Di Pasquale, "Simplex-coded BOTDA sensor over 120 km SMF with 1 m spatial resolution assisted by optimized bidirectional Raman amplification," Photon. Technol. Lett. **24**(20), 1823–1826 (2012).
20. X. Angulo-Vinuesa, S. Martin-Lopez, J. Nuño, P. Corredera, J. D. Ania-Castañon, L. Thévenaz, and M. González-Herráez, "Raman-assisted Brillouin distributed temperature sensor over 100 km featuring 2 m resolution and 1.2 °C uncertainty," J. Lightwave Technol. **30**(8), 1060–1065 (2012).
21. H. F. Martins, S. Martín-López, P. Corredera, M. L. Filograno, O. Frazao, and M. Gonzalez-Herráez, "Phase-sensitive optical time domain reflectometer assisted by first-order Raman amplification for distributed vibration sensing over >100 km," J. Lightwave Technol. **32**(8), 1510–1518 (2014).
22. M. A. Soto, X. Angulo-Vinuesa, S. Martin-Lopez, S. Chin, J. Ania-Castañon, P. Corredera, E. Rochat, M. Gonzalez-Herraez, and L. Thévenaz, "Extending the Real Remoteness of Long-Range Brillouin Optical Time-Domain Fiber Analyzers," J. Lightwave Technol. **32**, 152–162 (2014).
23. J. Pastor-Graells, H. F. Martins, A. Garcia-Ruiz, S. Martin-Lopez, and M. Gonzalez-Herraez, "Single-shot distributed temperature and strain tracking using direct detection phase-sensitive OTDR with chirped pulses," Opt. Express **24**(12), 13121–13133 (2016).
24. L. B. Liokumovich, N. A. Ushakov, O. I. Kotov, M. A. Bisyarin, and A. H. Hartog, "Fundamentals of optical fiber sensing schemes based on coherent optical time domain reflectometry: Signal model under static fiber conditions," J. Lightwave Technol. **33**(17), 3660–3671 (2015).
25. S. Sumida, S. Okazaki, S. Asakura, H. Nakagawa, H. Murayama, and T. Hasegawa, "Distributed hydrogen determination with fiber-optic sensor," Sensors Actuat B-Chem **108**(1), 508–514 (2005).
26. B. Culshaw and A. Kersey, "Fiber-optic sensing: A historical perspective," J. Lightwave Technol. **26**(9), 1064–1078 (2008).
27. S. M. Klainer, "Fiber optic which is an inherent chemical sensor," United States patent 4,846,548 (July 11, 1989).
28. H. H. Qazi, A. B. B. Mohammad, and M. Akram, "Recent progress in optical chemical sensors," Sensors **12**(12), 16522–16556 (2012).
29. B. Culshaw, "Optical fiber sensor technologies: opportunities and–perhaps–pitfalls," J. Lightwave Technol. **22**(1), 39 (2004).
30. J. P. Dakin, "Distributed optical fiber sensors," Proc. SPIE **1797**, 76–108 (1993).
31. W. R. Seitz, "Chemical sensors based on fiber optics," Anal. Chem. **56**(1), 16A–34A (1984).
32. M. Belal, M. Petrovich, N. Wheeler, J. Wooler, A. Masoudi, F. Poletti, S. Alam, D. Richardson, and T. Newson, "First Demonstration of a 2μm-OTDR and Its Use in Photonic Bandgap CO_2 Sensing Fiber," Photon. Technol. Lett. **26**(9), 889–892 (2014).
33. P. Russell, "Photonic Crystal Fibers," Science **299**(5605), 358–362 (2003).

Optics EXPRESS

34. I. Dicaire, "Optical Gas-Phase Frequency References Based on Photonic Crystal Technology," (2012).
35. A. D. Fitt, K. Furusawa, T. M. Monro, and C. P. Please, "Modeling the fabrication of hollow fibers: Capillary drawing," J. Lightwave Technol. **19**(12), 1924–1931 (2001).
36. T. Peng, T. Xu, X. Wang, Z. Liu, S. Dai, S. Liu, Z. Zhao, and Z. Pan, "Simulation and fabrication of micro-structured optical fibers with extruded tubes," Optik **127**(20), 8240–8247 (2016).
37. P. M. Dower, P. M. Farrell, and B C. Gibson, "Optimal refractive index design for an optical fibre-based evanescent field sensor," Systems & control letters **56**(9), 634–645 (2007).
38. M. Calcerrada, M. Fernández de la Ossa, P. Roy, M. González-Herráez, and C. García-Ruiz, "Fundamentals on new capillaries inspired by photonic crystal fibers as optofluidic separation systems in CE," Electrophoresis **36**(3), 433–440 (2015).
39. I. Dicaire, J. C. Beugnot, and L. Thévenaz, "Analytical modeling of the gas-filling dynamics in photonic crystal fibers," Applied optics **49**(24), 4604–4609 (2010).
40. W. C. Swann and S. L. Gilbert, "Pressure-induced shift and broadening of 1510–1540 nm acetylene wavelength calibration lines," J. Opt. Soc. Am. B **17**(7), 1263–1270 (2000).
41. T. L. Bergman, F. P. Incropera, and A. S. Lavine, *Fundamentals of Heat and Mass Transfer* (John Wiley & Sons, 2011).
42. J. Limpert, T. Schreiber, A. Liem, S. Nolte, H. Zellmer, T. Peschel, V. Guyenot, and A. Tünnermann, "Thermo-optical properties of air-clad photonic crystal fiber lasers in high power operation," Opt. Express **11**(22), 2982–2990 (2003).
43. M. A. Lapointe, S. Chatigny, M. Piché, M. Cain-Skaff, and J. N. Maran, "Thermal effects in high-power CW fiber lasers," Proc. SPIE **7195**, 71951U (2009).
44. P. R. Yoder Jr., *Opto-mechanical Systems Design* (CRC press, 2005).
45. A. S. Webb, F. Poletti, D. J. Richardson, and J. K. Sahu, "Suspended-core holey fiber for evanescent-field sensing," Opt. Eng. **46**(1), 010503 (2007).
46. T. Ritari, J. Tuominen, H. Ludvigsen, J. C. Petersen, T. Sørensen, T. P. Hansen, and H. R. Simonsen, "Gas sensing using air-guiding photonic bandgap fibers," Opt. Express **12**(17), 4080–4087 (2004).
47. C. M. B. Cordeiro, M. A. R. Franco, G. Chesini, E. C. S. Barretto, R. Lwin, C. H. Brito Cruz, and M. C. J. Large, "Microstructured-core optical fibre for evanescent sensing applications," Opt. Express **14**(26), 13056–13066 (2006).
48. F. M. Cox, A. Argyros, and M. C. J. Large, "Liquid-filled hollow core microstructured polymer optical fiber," Opt. Express **14**(9), 4135–4140 (2006).
49. H. Lehmann, H. Bartelt, R. Willsch, R. Amezcua-Correa, and Jonathan C. Knight, "Distributed gas sensor based on a photonic bandgap fiber cell with laser-drilled, lateral microchannels," Proc. SPIE **7653**, 76532W (2010).
50. C. Martelli, P. Olivero, J. Canning, N. Groothoff, B. Gibson, and S. Huntington, "Micromachining structured optical fibers using focused ion beam milling," Opt. Lett. **32**(11), 1575–1577 (2007).
51. D. N. Wang, "Micro-engineered optical fiber sensors fabricated by femtosecond laser micromachining," in *Imaging and Applied Optics Technical Papaers* (OSA, 2012), paper STu4F–1.
52. Y. J. He, "Novel D-shape LSPR fiber sensor based on nano-metal strips," Opt. Express **21**(20), 23498–23510 (2013).
53. G. Stewart, F. A. Muhammad, and B. Culshaw, "Sensitivity improvement for evanescent-wave gas sensors," Sensors Actuat. B-Chem **11**(1), 521–524 (1993).
54. Y. Zhang, C. Shi, C. Gu, L. Seballos, and J. Z. Zhang, "Liquid core photonic crystal fiber sensor based on surface enhanced Raman scattering," Appl. Phys. Lett. **90**(19), 193504 (2007).
55. C. Martelli, J. Canning, D. Stocks, and M. J. Crossley, "Water-soluble porphyrin detection in a pure-silica photonic crystal fiber," Opt. Lett. **31**(14), 2100–2102 (2006).
56. J. Henningsen and J. Hald, "Dynamics of gas flow in hollow core photonic bandgap fibers," Applied optics **47**(15), 2790–2797 (2008).
57. C. P. Yu and J. H. Liou, "Selectively liquid-filled photonic crystal fibers for optical devices," Opt. Express **17**(11), 8729–8734 (2009).
58. F. C. De Lucia, D. T. Petkie, and H. O. Everitt, "A double resonance approach to submillimeter/terahertz remote sensing at atmospheric pressure," IEEE J. Quantum Electron. **45**(2), 163–170 (2009).

1. Introduction

The field of chemical sensing is nowadays of great importance [1] in industry, security [2, 3], biomedical applications [4, 5], manufacturing processes and fuel transportation [6]. In particular, fiber-optic based chemical sensors have shown interesting properties either for the detection of specific gases in air [7–9] or chemicals in solution [10]. In a fiber-optic chemical sensor, the glass, dielectric fiber, conveys the measuring signal and typically serves as the support of the transduction material, keeping any required electronic component separated from the measurand substance. This kind of sensors is therefore more convenient than electronic sensors in some potential scenarios where electrical signals should be avoided: for example, if a dangerous or explosive gas is present in the monitored area, or if there is a strong electric field which could

Optics EXPRESS

spoil the information coming from the sensor by causing interferences on the measurement signal. In spite of these advantages, chemical sensing has found a remarkable barrier when it refers to distributed sensing. Distributed sensing consists in the possibility of realizing measurements along a continuous sensitive element, instead of over a discrete set of localized, independent detectors. This approach is often preferred when the number of monitored points is large, because it reduces costs, energy consumption, interrogation time and avoids multiple calibrations, also making the systems more simple from the point of view of deployment and maintenance. Extending this same principle for the detection, identification and quantification of chemicals would be of great importance for fields such as oil/gas extraction, where the presence of e.g. methane might have a critical influence in the green-house effect [11]. It is a common approach in these cases to use an array of several localized sensors in order to provide quasi-continuous chemical detection and monitoring over space [12]. However, these approaches do not represent a truly distributed sensing solution. Moreover, in systems where thousands of points need to be monitored, such arrayed configurations become extremely costly and, therefore, almost impossible to carry out.

In many other domains, distributed sensors have found major acceptance and have proven to be reliable and accurate [13–15]. Indeed, they are becoming a standard monitoring tool in industrial and technological environments, for instance assuring pipeline integrity [16, 17] or providing efficient structural health monitoring of large infrastructures. In terms of performance, experiments based on techniques as extended as Brillouin Optical Time Domain Analysis (BOTDA) or Phase-sensitive Optical Time Domain Refletometry (ΦOTDR) reach 2 m resolution along a distance range of 100 km [18] (which means 50,000 distinct resolved points in a single optical cable) or even more when combined with SNR-enhancing techniques such as coding [19] or Raman scattering [20–22]. Temperature resolutions of the order of mK [23] have also been achieved with measuring times in the order of 1 ms. In typical time-domain configurations, a light pulse is sent into the fiber, and a small fraction of the incident light is backscattered towards the emitter. The time of flight of the light pulse in the fiber gives the localization of the backscatter, and the analysis of the local backscatter might reveal information of certain thermal and mechanical fiber properties [24]. Distributed optical fiber sensors have, so far, been demonstrated to be well-suited for the sensing of physical quantities such as temperature or strain. Since the amount of scattered light is proportional to the incoming light, taking into account successive points along a fiber section, it is also possible to quantify loss or absorption.

Using these principles, there have been some demonstrations of fiber-based distributed chemical sensors but, to the best of our knowledge, they are all inherently limited. In some cases, they are necessarily supported by the use of a transducer coating on the fiber [12, 25–31], therefore lacking of an intrinsic chemical sensitivity. In these setups, the coating is delegate to perform the actual chemical detection, whereas the fiber sensor is aimed to quantify the change in a certain optical property of the fiber triggered by the transducer. Thus, the chemical sensitivity relies on an intermediate physical (mechanical, thermal, etc.) mechanism acting between the transducer and the fiber. Inevitably this approach leads to a strong *cross-sensitivity* of the sensor to environmental changes. Moreover, in these configurations, the fiber coating must be highly *selective* – it must provide a certain thermal or mechanical sensitivity to only a given substance – and generally requires to be somehow attached or embedded onto the optical fiber. Fulfilling both requirements simultaneously is particularly complicated or requires adapting sophisticated manufacturing methods on a case-by-case basis: if special coatings have to be used, they have to be modified according to the chemical to be detected. Thus, extending the concept to new substances is usually challenging and often impossible. In other configurations, the use of hollow/holey fibers allows the application of absorption spectroscopy [32] (for an updated review see Ref. [8]), which renders these methods highly selective. However, these approaches generally fail to show long sensing ranges due to the inevitable trade-off between loss and distance range. In these cases, the fiber loss (which limits the range) is not something to minimize, but actually required to

Optics EXPRESS

perform the measurement. Moreover, they require working with instrumentation that is not as well developed as conventional optical fiber instrumentation at 1.55 μm.

In this work we propose a new scheme to perform fully distributed, spatially-resolved detection of gas species along a holey optical fiber with spectroscopic selectivity and suitable for a variety of chemicals with a single configuration. The new method is based on realizing wavelength-modulated photothermal spectroscopy in a microstructured optical fiber (MSF), and probing the resulting heat distribution along the fiber using a dynamic distributed temperature measurement system with mK resolution. In our scheme, the evanescent field escaping the core of the fiber due to a propagating continuous wave (CW) signal is used to thermally excite the target chemical species, present in the close vicinity of the fiber core. When tuned on a gas molecular absorption line, the laser light is absorbed and the gas is heated by non-radiative molecular relaxation. The temperature changes along the fiber are determined with a fast and high-resolution distributed sensor based on chirped-pulse reflectometry [23]. Although phase-sensitive optical time domain reflectometry has previously been suggested for gas sensing [9], our work represents the first time that such a distributed photothermal measurement is actually experimentally demonstrated. Moreover, the system proposed here does not require a *coherent detection* setup, like the one proposed by W. Jin et al. Wavelength modulation in the heating laser allows to easily discriminate the ambient temperature variations from the actual presence of gas. Like previous demonstrations, the use of molecular absorption lines provides the system with spectroscopic selectivity and reduced cross-sensitivity. However, since the measured quantity is the temperature, the vast majority of the system can work as a conventional distributed temperature sensor, i.e. the majority of the system components can operate at the conventional telecom window of 1.55 μm. The system can thus potentially reach the performances of range and resolution already demonstrated in previous configurations.

Throughout the whole manuscript, a proof-of-concept experiment of this idea based on the use of a conventional index-guiding MSF is explained and the results obtained are shown. The proposed method represents a strong potential for the development of distributed gas sensors, provided that specific fibers, optimized for our aimed application, become available.

2. Working principles

2.1. Basic concept

For the proof-of-concept, we used a gas-filled index-guiding microstructured fiber to perform the demonstration. MSFs are a special family of fibers characterized by having hollow conduits following a regular pattern along their cross section. This pattern is usually achieved by stacking and drawing multiple glass rods and hollow tubes while they are fabricated [33]. This way, the fiber is formed by a succession of different regions occupied by glass or vacuum/gas that run along the whole fiber. In most small-core MSFs, the evanescent field of the guided mode shows a certain overlap with the gas-filled holes, thereby allowing a non-negligible interaction between the guided light and the gas, which is here exploited for sensing purposes. In this work, an approximately 10 m long MSF with a hexagonal lattice structure was used as the sensitive element of the system. The SEM photograph of the fiber cross section is shown in Fig. 1 (left).

For our experiment, we used an acetylene-filled all-fiber gas cell [33, 35–38]. To fabricate the all-fiber gas cell, one end of the MSF is first fusion-spliced to a short segment of ultra high numerical aperture fiber plus a standard single mode fiber using a tailor-made splicing program. The pigtailed MSF is then placed in a hermetic gas chamber for air evacuation followed by gas filling of the holes of the MSF at a targeted low pressure with the desired gas sample. The last step involves a similar fusion splice procedure at the other end to hermetically seal the MSF. To prevent air contamination in the filled MSF, the latter is loaded with helium at high pressure (above atmospheric pressure) before being taken out from the gas chamber, such that this slight helium overpressure prevents air from entering in the fiber holes during the final splice. Within

Optics EXPRESS

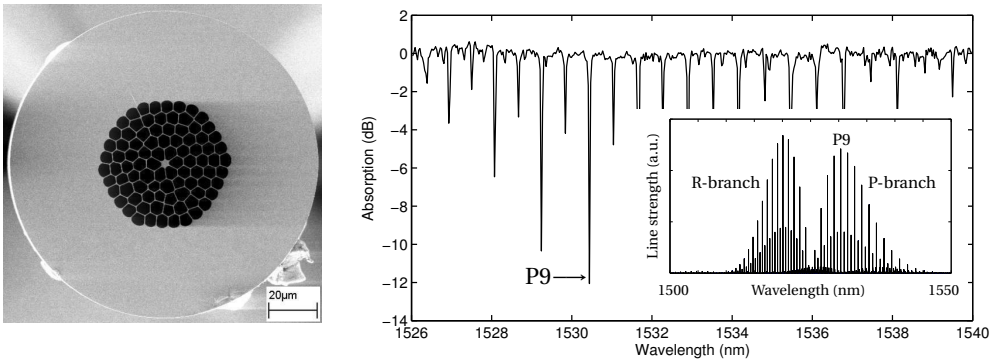

Fig. 1. Left: SEM photograph of the index-guiding MSF cross section structure [34]. The black bar is 20 μm long; Right: Optical Spectrum Analyzer (OSA) measurement of a wide band light source absorption in acetylene; Inset: line strength along the whole acetylene rotational-vibrational branches (HITRAN database) [34, 40].

several hours, the helium diffuses out of the fiber due to its high permeation coefficient through silica, leaving only the low-pressure gas inside the cell. The whole fabrication process is fully described in [39]. Figure 1 (right) shows the absorption spectrum of the fiber, where the acetylene gas resonances can be appreciated. The filling pressure was around 70–75 mbar. Considering this, we can deduce a theoretical linewidth for a given peak. However, the fiber cell employed shows an additional, slight linewidth broadening due to the small size of the holes. The best way to determine the actual linewidth is therefore through direct measurement, which was performed by analyzing the cell transmission spectrum with a high-resolution Optical Spectrum Analyzer (OSA). This measurement, shown in the Fig. 2, gave a FWHM value around 1.5 GHz for the line of interest in this experiment (P9).

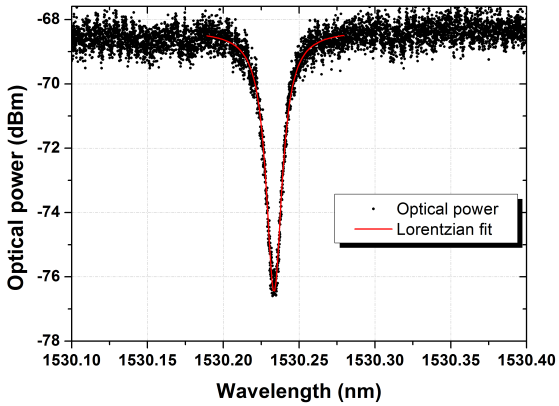

Fig. 2. P9 acetylene transition peak measured in the all-fiber gas cell using a high-resolution (10 MHz) OSA using a wide band light source at the gas cell input.

The temperature distribution along the fiber core was monitored continuously and dynamically with high temperature resolution using a chirped-pulse ΦOTDR system [23]. Chirped-pulse-ΦOTDR systems are able to provide, in the best conditions, single-shot determination of mK temperature changes along an optical fiber. In a chirped-pulse-ΦOTDR system, every pulse has the same linearly-varying instantaneous frequency profile, resulting in traces with local delays proportional to the local temperature or strain gradient experienced by the fiber. The shot-to shot

Optics EXPRESS

temperature or strain changes are thus recovered by computing the trace-to-trace local correlation shifts among the different trace sections. This single-shot characteristic of chirped-pulse-ΦOTDR is the key point potentially allowing a fast-response chemical sensor. We will see later that this fast response allows discriminating the photothermal response, caused by the gas heating, from the regular temperature changes caused by temperature fluctuations. The spatial resolution provided by the system in this case is 2 meters (20 ns pulse). With the chirp value used in this case (65 MHz/ns) and the digitizer resolution (40 GSPS), the temperature resolution provided by this method is in the order of 2 mK. The readout time for a length of 10 meter is in the sub-second range (50 ms), even considering the relatively high ($N = 32$) number of averages used.

At the same time, a laser source tuned around the P9 line (~1530.2 nm) of the acetylene gas spectrum shown in Fig. 1 (right) was used as a heating pump in order to induce photothermal heating in the gas upon absorption. As the gas temperature increases, heat is transferred to the fiber core, producing a small but detectable change in its temperature. The temperature change that can be induced by photothermal absorption in this volume is in the order of hundreds of mK, as we will show below. This is comfortably measured using the chirped-pulse ΦOTDR method described above. Since the heating is proportional to the gas concentration, this procedure should in principle allow mapping the concentration of a target gas along the fiber with high spatial resolution. We demonstrate hereafter that this idea has some limitations given by the fiber homogeneity, and possibly calibration procedures should be put forward to turn this concept into a feasible technique. Nevertheless, even in its current form, the system is able to determine the presence of a target gas with spectroscopic selectivity, which is particularly interesting in the field of chemical sensing, without the need of specifically-coated fibers. As it is based on the use of a ΦOTDR system, it can be potentially extended to long-range detection applications, provided there is a fiber able to guide light at both the gas absorption wavelength (typically in the mid-infrared) and the interrogation wavelength, typically around 1.55 μm.

2.2. Heat model

In our case, an index-guiding MSF containing a gas analyte was used. This analyte is heated by the evanescent field of an external optical pump traveling along the core. Part of the heat is transferred to the fiber core by thermal conduction, whereas the ΦOTDR signal (at a different wavelength) is simultaneously scanning the temperature changes. It is important to obtain a preliminary evaluation of what are the required parameters (particularly heating pump power and temperature resolution of the ΦOTDR setup) to make the concept work. For this, we developed a simple model of the thermal response of our MSF fiber when exciting the acetylene molecules inside it. As a basis, we take into account the structure shown in Fig. 1 (left).

Ideally, a fraction P_{abs} of the optical power being pumped into the fiber (P_{pump}), is going to be absorbed by the gas inside it. Therefore, this power is going to be converted into heat by non-radiative molecular de-excitation . Considering the possibilities for the heat to be transferred, the following power balance equation will be satisfied:

$$P_{\mathrm{abs}} + P_{\leftarrow \mathrm{s}} = P_{\rightarrow \mathrm{s}}, \tag{1}$$

where $P_{\rightarrow \mathrm{s}}$ and $P_{\leftarrow \mathrm{s}}$ are the power exchanges between the fiber and its surroundings. The radiative exchange can be neglected in this system, as its magnitude is not in the scale of the convective contributions for the low temperature differences intervening [41]. Consequently, the starting equation is reduced to:

$$P_{\mathrm{abs}} \approx P_{\mathrm{conv}}, \tag{2}$$

P_{conv} being the convective heat loss. Due to law of conservation of energy, this is indeed the power crossing any arbitrary cylindrical surface in our system.

Upon illumination, and after a short transient, a steady state should be reached for the core temperature. After the steady state has been achieved, the power flux going out of the fiber due

Optics EXPRESS

to the spontaneous convective air currents around its external surface S_e is given by the law of convection [41]:

$$\frac{P_{conv}}{S_e} = h\,(T_e - T_s), \tag{3}$$

where h is the convective coefficient, T_s is the temperature of the surroundings (static) and T_e the external temperature of the fiber coating (assumed homogeneous and steady). The combination of Eq. 2 and Eq. 3 gives the temperature difference between the fiber coating and the surrounding air.

In order to reach a reasonable prediction of the scale of the temperature changes to be induced by the pump when acting on the gas, we are constrained to do estimations about the value of some of the involved parameters. This is important to make sure that our ΦOTDR system is a suitable distributed thermometer for the proposed application, and to establish the appropriate range of pump power to be used.

The first necessary estimation is the fraction of guided light which is propagating out of the core and through the acetylene. This fraction depends essentially on the optical mode overlap with the cells where the gas is confined, and will have a direct impact on the gas absorption per meter along the fiber. Considering the SEM photograph of the cross section of the fiber shown in Fig. 1, the mode overlap with the gas can be calculated using finite element methods, and results to be in the order of 3.8% at 1.5 μm. With the absorption cross section of acetylene for the P9 line and the pressure used, this gives a total absorption of ≈ 1 dB/m, which is in good agreement with the measured losses at this gas resonance. The insertion loss of the fiber out of gas resonance was also measured to be ∼15 dB, and the loss due to each splice is estimated to be ∼3 dB. This means there is a *background loss* due to scattering of light out of the fiber which is around 1 dB/m. Considering these loss factors and the 1dB/m absorption at the P9 resonance, we can estimate the power absorbed at the first meter of the fiber to be about 30 % of P_{pump}. With these figures and a pump power of ∼100 mW, we can estimate the amount of dissipated power in the first measured fiber meters, which for our setup can reasonably reach the range of tens of mW/m. As the absorption along the fiber modifies the value of dissipated power along the fiber, we will only consider the problem for the first meter of the MSF (which is assumed homogeneous along the propagation distance). The power dissipated beyond this first meter will decay at a rate of 2 dB/m approximately, according to our characterization of the fiber.

An estimation of the external surface of this first meter of fiber is also required in the calculations. The diameter of the protective acrylate coating of the fiber is comparable to the standard SMF sizes. Taking a value of $R_e \approx 125$ μm for the external radius of this coating, the corresponding surface would be $S_e \approx 8$ cm^2 (per meter length).

Finally, we have to choose a value for the convective coefficient. This coefficient is usually in the range from 2 to 25 $\frac{W}{m^2K}$ for non-forced convection [41, p. 8]. If we choose an intermediate value of $h \sim 15\frac{W}{m^2K}$, we can calculate the temperature difference between the fiber surface and the surrounding atmosphere, assuming its temperature is 300 K. The result is approximately 2 mK per mW pumped into the MSF (P_{pump}).

We can now consider the conduction of heat from its source in the gas cells around the core, and apply a similar analysis to the ones developed in the references [42, 43]. To model it, we take the physical dimensions from the SEM image of the fiber (Fig. 1 (left)) and assume a simplified scheme like the one shown in Fig. 3 (left). Due to the relatively small transversal dimensions, the longitudinal heat conduction can be neglected. Thus, the calculation will be based on heat transfer through a composite structure consisting in a set of cylindrical shells with different radii: a glass core; five *holey glass* layers; a solid glass cladding layer; and a solid acrylate external coating shell. Heat transport is characterized in each material by a different thermal conductivity (k).

Given the geometrical and thermal properties of the structure, we can use *Fourier's law* to study heat conduction. This law is easily applied to our radial heat conduction problem, particularly in

Optics EXPRESS

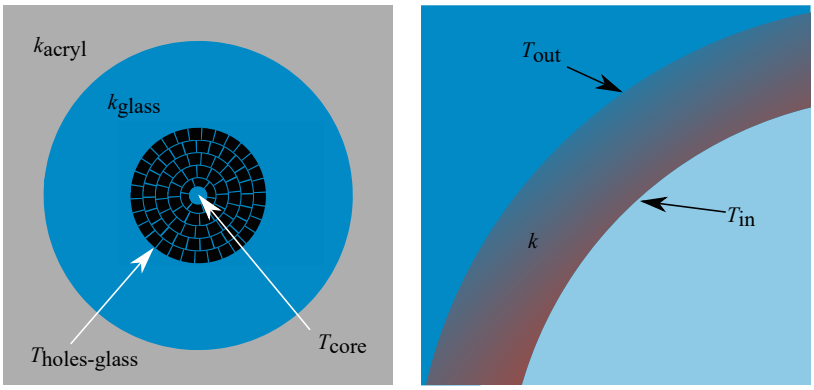

Fig. 3. Left: simplified cross section employed to model the steady temperature distribution of the MSF (not to scale); Right: scheme showing the general notation used for an arbitrary cylindrical shell within the structure. The heat flow across it is described by Eq. 4.

the external, solid layers of our fiber (acrylate and solid glass). The heat flow through each of these shells (Fig. 3 (right)) establish a temperature gradient across it which also depends on its thickness and thermal conductivity k. Considering the net power being transmitted through any cylindrical surface enclosing the fiber is P_{abs}, we can directly integrate Fourier's law and solve for the temperature at the inner face (T_{in}) of a given shell obtaining:

$$T_{in} = T_{out} + \frac{P_{abs}}{2\,\pi\,L\,k} \log\left(\frac{R_{out}}{R_{in}}\right). \tag{4}$$

Here T_{out} is the temperature at the outer face of the considered shell, and R_{in} and R_{out} are the radii of its inner and outer surfaces, respectively. Taking the obtained temperature at the external surface of the coating as boundary condition, and the corresponding parameters for each solid shell ($k_{acryl} \approx 0.20$ and $k_{glass} \approx 1.37\ \frac{W}{Km}$ [44]) we get a temperature $T_{holes-glass}$ just outside the holey region which is only 0.01 mK above the acrylate/air interface (per mW pumped into the fiber). Therefore, we can consider the effect of outer glass cladding and coating as negligible. This implies that the temperature at the outer boundary of the holey structure is essentially equal to the environmental temperature. It should be noted that, in our model, we do not consider temperature drops at any of the interfaces between glass and acrylate owing to the advanced fabrication techniques usually employed nowadays [43].

To calculate the temperature at the fiber core, where the ΦOTDR system will be measuring it, we neglect the radial conduction in the thin cylindrical walls separating each holey shell. We will also neglect heat transmission through the holes. According to our estimations, even at atmospheric pressure, conduction through the gas should be around 100 times less effective than conduction through the solid glass. If we consider the angular ratio of glass and holes in the structure and apply Fourier's law, we find that the heat transfer in the bridges should be some ≈ 10 times larger than in the holes. This is enough to discard, in a first approximation, the heat conduction through the holes. Thus, heat is only being transferred through the holey shells by means of conduction along a series of solid glass bridges of length $\Lambda \approx 5$ μm. For each one of these five shells, heat transfer is distributed between a different number (n_i) of bridges, which, for simplicity, are all considered to have equal and homogeneous thickness ($\tau \approx 0.4$ μm). In this region, then, the conduction problem is no longer radial, but Cartesian. Under this assumption, and considering all the holey shells, the solution to the heat equation can be written down as:

$$T_{core} = T_{holes-glass} + \frac{\Lambda\,P_{abs}}{L\,\tau\,k_{glass}} \sum_{i=1}^{5} \frac{1}{n_i}, \tag{5}$$

Optics EXPRESS

where T_{core} is the temperature of the fiber core and $T_{holes-glass}$ the previously calculated temperature at the interface between the holey shells and the solid glass shell. With this expression, we can estimate that the temperature in the fiber core is 0.1 mK higher than the one at the outer surface of the fiber (per mW pumped into the fiber). Thus, overall, the core heating is controlled essentially by the acrylate/air interface. Beyond that, the main internal drop of temperature is located at the interface between the holey shells and the glass cladding. This result is consistent with the conclusions of the reference [42]: the distribution of temperature is governed mainly by the coating-air interface.

In summary, we finally find an order of magnitude estimation of the scale factor between the input power (P_{pump}) and the expected core temperature. Considering all the variables above, this is approximately 2 mK of temperature elevation in the core per mW pumped into the fiber. Considering that hundreds of mW can easily be pumped into the fiber, we assume that our system should be capable of measuring these temperature changes.

This proves that our ΦOTDR system should theoretically be able to detect the temperature changes induced by the pump laser on the gas. This will be experimentally demonstrated in the following sections.

3. Experimental setup

A tunable distributed feedback (DFB) CW laser source emitting at the wavelength of the P9 acetylene line with a linewidth of ~10 MHz was chosen as heating pump. The laser can be digitally tuned with a tuning resolution of 1 pm. The laser output was amplified and fed into the MSF through one of the ends of the 10 m long MSF. The power of the heating pump was controlled by means of a tunable attenuator, while a fraction of 1 % of the input power was used for monitoring purposes in an optical power meter (PM) (Fig. 4).

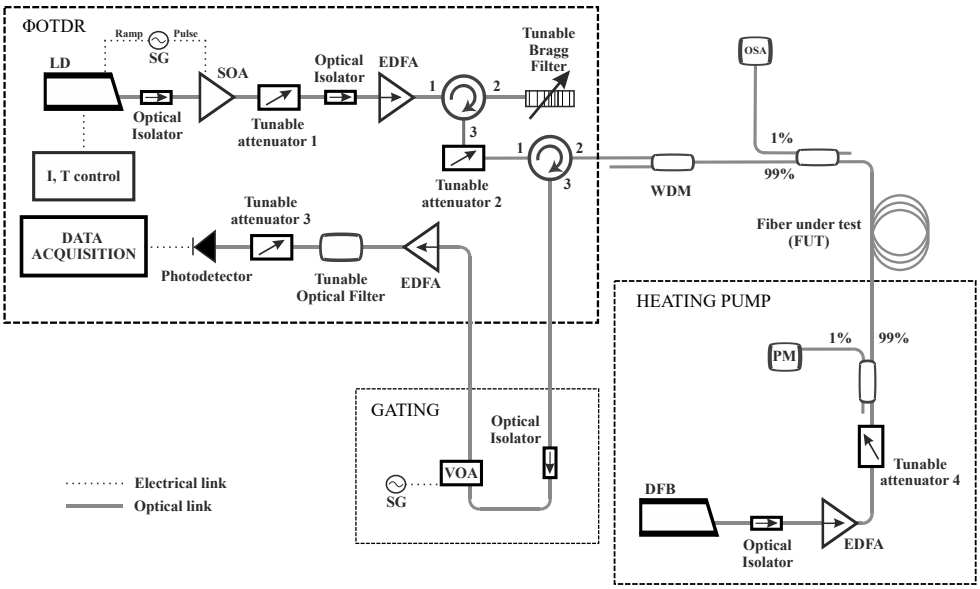

Fig. 4. Scheme of the experimental setup employed. Acronyms are explained within the text.

The pump was also monitored (1 %) at the output end of the gas-filled fiber allowing us to check in an OSA whether it is being absorbed or not by the acetylene resonance lines. An appropriate Wavelength-Division Multiplexer (WDM) was used to filter out the pump to prevent it from

Optics EXPRESS

reaching the ΦOTDR system, while allowing the passage of the pulsed signal to interrogate the fiber under test (FUT).

The chirped-pulse-ΦOTDR probe pulse was sent from the opposite end of the FUT to monitor the temperature of its core. The scheme used is very similar to the one depicted in our previous reference [23], comprising a modulated DFB laser diode (LD) to generate the chirped response and a Semiconductor Optical Amplifier (SOA) driven by a signal generator (SG) to carve the desired pulses. Overall, the pulses obtained are 20 ns width (2 meter spatial resolution) and show a highly linear chirp response (total spectral response is 1.3 GHz). With these values of chirp and pulse width and considering the performances of our digitizer (40 GSPS), the temperature resolution obtained is around 2 mK. The pulse repetition rate was 4 kHz, and each final trace was averaged 32 times, allowing us to properly measure the temperature every 50 ms. The pulses are then amplified by means of an EDFA, whose input is attenuated in order to avoid generating nonlinearities. After filtering the amplified spontaneous emission (ASE) produced in the EDFA with a tunable Bragg filter and controlling the final pulse power with another tunable attenuator, the pulse is launched into the FUT through a circulator. The generated Rayleigh backscattering is then collected, amplified and filtered in order to have a clean signal reaching the photo-detector. The ΦOTDR signal showed strong reflections caused by the splices between the MSF end and the input standard fiber, which were strong enough to completely screen the trace afterwards. To eliminate them, a gating stage comprising a MEMS fast switch synchronized with the SOA was required in detection. The delays in the synchronization control were carefully chosen to maximize the amount of trace visible in the detector. This is also the reason why the pump was chosen to counterpropagate, allowing us to properly make temperature measurements at the pump input end, where more power is dissipated and therefore higher contrast in the measurement results should be expected. For all results presented in this paper, positions along the fiber (z) are always referred to the heating pump input end as origin.

4. Results

First of all, we observed the heating dynamics in the fiber core as a function of the different optical inputs into the fiber. From these observations, two heating contributions were found. They were discernible thanks to their different time response and magnitude of the heating. These heating regimes correspond to the pump laser being on and off-resonance. The dynamics of a typical experiment are summarized in Fig 5, where the heating pump is switched on first (off-resonance), subsequently driven into the gas absorption resonance, driven off-resonance again and finally switched off completely. As it can be seen, there is a slower (and larger in magnitude) contribution when the pump is off-resonance, and another faster and smaller in magnitude when the pump is on-resonance. The slowest contribution (starting at $t \approx 1.5$ min and continuing until $t \approx 5.2$ min) is presumably associated to the absorption of scattered light in the fiber coating, and due to the 1 dB/m background loss aforementioned. The origin of this contribution lies in the large scattering loss of these fibers. All the scattered power from the fiber core is absorbed in the plastic coating of the fiber. This absorbed power heats the coating and transmits some heat to its core, raising the temperature. This contribution is independent of the wavelength of the pump since the absorption in the fiber coating is broadband. The other contribution was much faster (it develops its full temperature change in roughly half a minute from $t \approx 3.5$ min) and only present when the pump wavelength was tuned on-resonance with the P9 acetylene absorption line. Thus, the ΦOTDR system is able to quantify the relevant changes in fiber temperature related to the presence of the gas in the holes of the MSF, potentially allowing to detect it. It is worth to mention the fast beginning of the background temperature increase, which is steep enough to be associated to the gas absorption in the fiber. A probable hypothesis for this is that the gas is being heated by the ASE coming from the EDFA which amplifies the CW pumping signal, as it could be exciting some of the gas resonances adjacent to the P9 line.

Optics EXPRESS

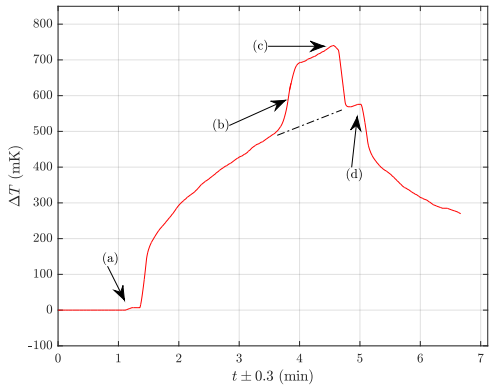

Fig. 5. General thermal behavior of the acetylene-filled MSF (at $z = (1.3 \pm 1)$ m) when the pump is: (a) switched on (laser off-resonance plus EDFA); (b) tuned on-resonance; (c) tuned off-resonance; (d) switched off ($P_{\text{pump}} \approx 70$ mW). A smoothing filter has been applied.

In order to eliminate the effect of the slow contribution on the temperature measurements and possible ΦOTDR laser wavelength drifts, a periodic wavelength modulation of the heating laser was made. This modulation was generated by adding a ~1 mA amplitude sine oscillation with a frequency of 0.5 Hz to the DFB bias current. This additional current corresponds to a peak wavelength displacement of about +(6 ± 1) pm. The wavelength dithering must be slow enough for the thermal dynamics to follow it, as the reason for this modulation is to identify the analyte by means of a temperature evolution correlated to the wavelength dither of the heating laser. Considering the (relatively slow) temporal response of the gas heating, the modulation frequency has to be set in the range of several Hz. The measurement shown in Fig. 6 (left) was made starting the temperature acquisition with the pump wavelength oscillating around the resonance line. After some minutes, the central wavelength of the oscillation was driven out of resonance. As it can be seen, tuning the laser off-resonance makes a large step change in temperature, both in average heating and in the superimposed modulation. Interestingly, although the laser wavelength is still oscillating, no temperature modulation is observed, confirming that the background heating comes from a broadband absorption mechanism.

To clarify the presence of the modulation subject to the proximity of the absorption line, two windows of 4 and 8 minutes were taken from the temperature evolution in Fig. 6 (left). The segments were chosen respectively from the lapses in which the pump was “on-resonance” and “off-resonance”. The Fourier transform of each segment was computed, and the results appear in Fig. 6 (right). The resulting curves show that the induced oscillation frequency (0.5 Hz) together with its first harmonics appear only when the pump is on-resonance, and disappear completely off-resonance. The dynamic range of the system over this measurement period (several minutes) is >10 dB. It should be noted that the temperature measurements were done at the point $z \approx (1.3 \pm 1)$ m.

These results also prove the feasibility of separating the contributions arising from the photothermal response from the background temperature fluctuations in the fiber.

It is important now to observe the behavior of the system as a function of the fiber length. To do so, the fiber heating was mapped along both t and z in order to show the convenience of the method to develop a functional distributed optical fiber gas sensor. Two of the resulting maps are shown in Fig. 7. The first one was registered when the pump laser source was tuned on-resonance with the P9 line (~1530.2 nm). The second one corresponds to the same experiment but when the pump was off-resonance. The fiber was allowed to reach a homogeneous room temperature

Optics EXPRESS

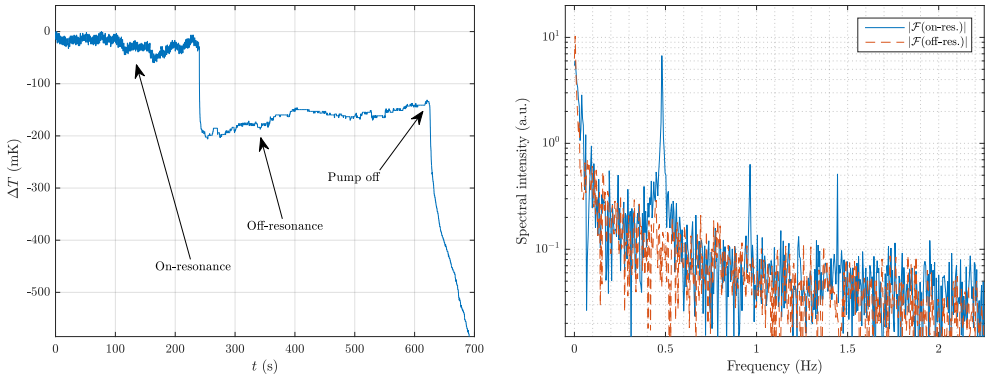

Fig. 6. Left: temperature changes produced by the pump being modulated around and off-resonance ($P_{\text{pump}} \approx 105$ mW); Right: Fourier spectrum of the signals extracted from different time intervals of the temperature changes curve showing the induced modulation when it was active.

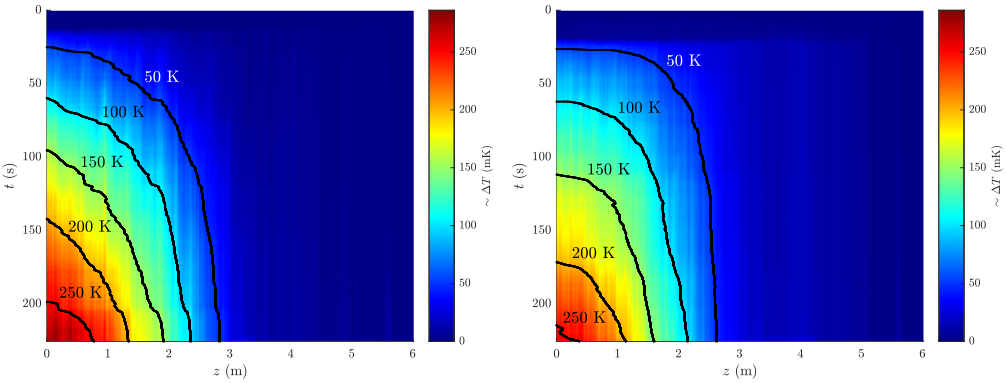

Fig. 7. Heating $z - t$ map obtained when the pump is turned on (at t = 15–20 s, $P_{\text{pump}} \approx$ 105 mW): Left: on-resonance; Right: off-resonance.

before performing the experiment.

The maps show the expected exponential Beer-Lambert behavior in z, corresponding to the loss of pump power along the distance. The temperature change is directly proportional to the power being dissipated at each point of the fiber, which also decays exponentially due to the pump losses. The losses in our case originate not only from the absorption of the gas species but, as commented before, from the large scattering losses in this fiber. This loss also sets an inevitable range limit to the sensor. In our case, considering the total losses at the pump wavelength, the available heating input power and the temperature resolution of the ΦOTDR system, the dynamic range of the system does not exceed 15–20 dB. Correspondingly, this sets a distance limit of approximately 10 meters in the total fiber length of this type that can be monitored. However this is not a limit of the technology, but rather a limit of our own setup.

It should be noted that these on-off thermal maps show the aggregate response of the coating and photothermal responses. A more careful measurement, able to undoubtedly discriminate between the thermal responses of cladding and acetylene, was performed with the aforementioned wavelength modulation around the resonance wavelength. This wavelength modulation unequivocally resolves the gas absorption from any other temperature contribution either coming from a

Optics EXPRESS

broadband absorption within the fiber (such as the observed cladding absorption of scattered photons) or from simple ambient fluctuations. In this case, the modulation was done at 0.25 Hz. A Fast Fourier Transform was calculated for every z, considering the temporal evolution of the temperature along a time frame of 780 seconds. The results are shown in Fig. 8 (left). As it can be seen, the peak at 0.25 Hz appears all along the fiber, demonstrating the range of the technique. The

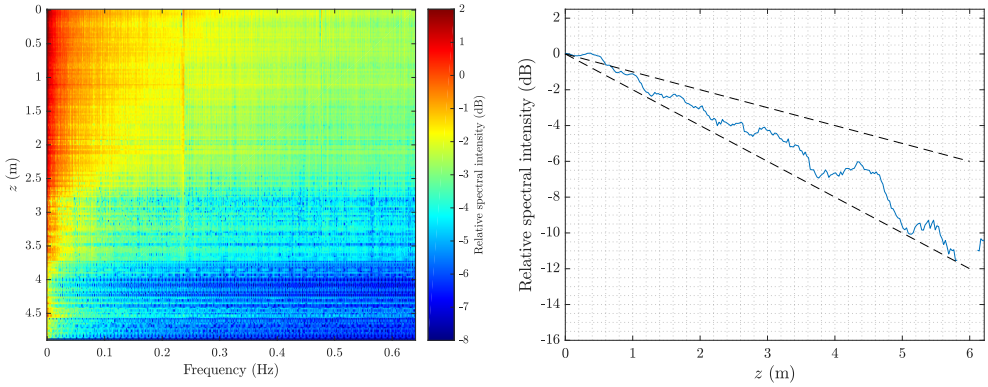

Fig. 8. Left: map showing the intensity of the induced thermal modulation for each driving frequency along the first meters of the fiber ($P_{\text{pump}} \approx 110$ mW); Right: a slice of the map around the modulation frequency (0.25 Hz) traces an approximately exponential temperature decay along the fiber. The dashed lines indicate the maximum and minimum expected decays.

amplitude of the 0.25 Hz peak was traced along the distance and is represented in Fig. 8 (right). The minimum expected decay rate corresponds to the background loss, which would result in a 1 dB/m slope in the curve. But there is an additional $\leq$ 1 dB/m loss due to absorption in the gas that will affect the pump signal every time it gets closer to the P9 resonance wavelength. Thus, the slope of the curve should be close to 2 dB/m and not less than 1 dB/m. Both limits have been represented in Fig. 8 (right) by dashed lines. Although the general evolution of the temperature amplitude is exponentially decaying, it can be seen now that there are non-uniformities in the heating process. This is probably a result of the changing geometrical characteristics of the fiber along its length [30], which lead to a varying overlap between the optical mode and the gas and correspondingly a different heat dissipation along the fiber axis. This causes variations in the temperature response as a function of the distance. In principle, these variations could be accounted for with a suitable calibration procedure (e.g. pre-filling the whole fiber with a known gas concentration and measuring the response), though deploying this calibration procedure might be rather costly in general. This highlights the importance of having a different kind of fiber, where the microstructure would provide a greater and homogeneous overlap between light and gas. This could be achieved in a hollow-core fiber or in fibers with a optimized design for a larger evanescent field [33, 45–48]. However, for the best ΦOTDR response, it might be convenient to have a solid core, given the thermal dependence of refractive index in silica. Thus, it seems that fibers combining a hollow and a solid core could be the best option in this case. Such fibers are not widely available now, but might be in the future if this technique appears to be attractive enough. In summary, a fiber capable of guiding specific wavelength ranges in the IR (corresponding to gas absorption wavelengths) while showing also good transmission behavior and temperature sensitivity at 1.55 μm is required for the proposed method to work as a distributed long-range gas sensor. Different chemical species could be distinguished and their concentrations mapped quasi-simultaneously by simply changing the operating wavelength of the pump to the corresponding transition line for each analyte.

As a final test, we decided to calibrate the temperature variation recorded in the fiber as a

Optics EXPRESS

function of the pump power entered in the the MSF. According to the model, the temperature raise in the fiber should scale linearly with the input power, since the dissipated power is proportional to the input power. The measurement of this response would allows us to determine the sensitivity of the method as a function of the power pumped inside the sensing fiber. To do this, the wavelength of the pump was set on-resonance for different output powers. After having reached a static temperature trend, the pump was suddenly tuned off-resonance. The consequent response at $z \approx (1.3 \pm 1)$ m is shown in Fig. 9 (left). The temperature decrease at that point of the fiber was

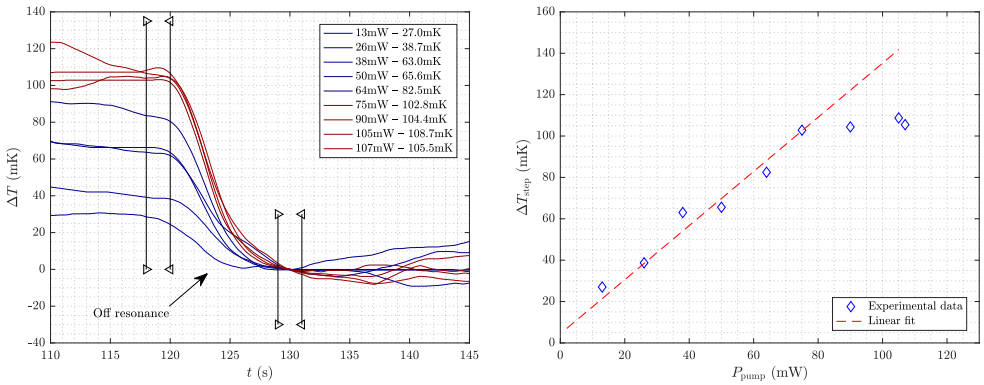

Fig. 9. Left: thermal response at $z \approx (1.3 \pm 1)$ m, for different pump powers, when going from on to off-resonance. Vertical lines mark the regions used to calculate each ΔT_{step}. A smoothing filter has been applied; Right: relation found by measuring the different steps height, and linear fit of the first 6 values.

then measured by taking the mean value of the curves in the regions marked with vertical lines in the figure and defining *temperature steps* ΔT_{step} for each pump power as the difference among the mean values in each segment. We used these steps to generate the calibration graph shown in Fig. 9 (right). The figure shows the expected linear response although a saturation of absorption is observable at high input pump power, compatible with the expected saturation intensity in these acetylene transitions. A consistent result has been achieved when comparing these values with the initial estimations obtained from the heat model, given the multiple unknown parameters (specifically considering the possible variations in the expected geometry, h parameter, pump-gas overlap, etc.). The experimentally obtained temperature raise of 1 mK per pumped mW in the fiber core was in fair agreement with the theoretical estimation of 2 mK/mW, particularly considering that many parameters such as the convective coefficient are roughly estimated.

The saturation obtained when pumping beyond the 80 mW range seems to indicate that there is a limit in the attainable sensitivity with this technique. To go beyond this limit, all the strategies should be focused on improving the fiber design to maximize the power dissipated in the gas.

5. Discussion

The results above prove that there is some potential for the development of distributed optical fiber gas sensors based on the photothermal effect. This method has several advantages over other configurations, among them the avoidance of specific coating/cabling elements and the possibility of having the vast majority of the system working at conventional telecom wavelengths (since the interrogated quantity is the temperature). Taking advantage of the characteristic spectra of different substances, the photothermal wavelength may be tuned to specifically detect and quantify the presence of multiple chemical species. On the other hand, the demonstration presented here shows several limitations, most of them related to the MSF used. In order to implement the method into an operative sensor of gas concentration, it would be necessary to characterize its

Optics EXPRESS

sensitivity at every point along the fiber by performing a calibration relating the concentration inside the sensing fiber and the heating produced. This should be done for a given pump power using one of the resonances of the sample gas. For each analyte, the calibration should also consider the amount of power able to reach each fiber position z_i, which is related to the amount of loss produced on the heating pump along $z < z_i$. Losses here refer to propagation loss and analyte-induced loss. The response and sensitivity along the fiber in a field implementation of the sensor would also be affected by the particular characteristics of the environment or the monitored structure, such as inevitable fiber bendings. Thus, an appropriate weighting should be done in the acquired temperature maps to take into account every factor and convert it to a concentration map of a particular analyte. These calibrations would require multiple cells with gas at different pressures or an open-to-air fiber and a setup similar to the one depicted in the reference [45].

Another important point that requires careful consideration in this system is the trade-off between the sensitivity of the measurement, requiring a strong absorption in the gas, and the sensing range, requiring a low absorption in the gas to have a longer reach in the heating pump. In any case, the use of a high pump power, mandatory for long range measurements, will always find limitation due to the observed saturated absorption by the gas. A dynamically tunable pump power may then be considered. It would help, for example, when facing applications that aim at different range scales, where a quantification might be required in relatively distant positions along the fiber. In such a case, the heating pump power could be tuned depending on the point of the fiber to be monitored in each situation, as it may not be a problem to reach absorption saturation along a previous segment of the fiber. What is important is just to have a linear response with the pump power in the region of interest to be monitored in each case. In addition, this would allow to accomodate the heating pump power to the concentration of target analyte that is observed in each case.

As aforementioned, one major issue when designing a sensor based on the demonstrated principle is the choice of an adequate probe fiber. On one hand, it should exhibit convenient guiding properties at both pump (target analytes spectra) and probe wavelengths, as well as enough overlap of light mode and the volume occupied by the sample; On the other hand, the fiber structure should maximize the exchange with the surroundings, in order to really sense the ambient and not just the gas filled into the fiber through artificial means. Higher pump-gas overlap may be obtained in more convenient kind of gas-filled fibers, such as a hollow-core fiber or fibers with a optimized design for a greater evanescent field [33, 45, 47, 48]. New experiments in these fibers should provide some more insight into the studied method prospects and possible applications. Simultaneously, the searched fibers should also exhibit a measurable temperature sensitivity of the effective refractive index at 1.55 μm. These two restrictions might not be easy to achieve in a single fiber core.

Although the results shown in this work have demonstrated the validity of the idea without the need of a tailor-made sensing fiber, a new structure with separate guiding mechanisms could be implemented to achieve the guidance of the heating laser and the conventional temperature probing at 1.55 μm. In other words, the heating wavelength and the temperature probing wavelength should not necessarily travel through the same core, it is simply needed that the temperature change of one core is seen by the other core. Given the heat dynamics of an optical fiber, it seems clear that such a condition is easy to meet, with the usual dimensions and materials used. This brings a large flexibility in the design, as the two cores can be designed independently for the best guiding performance of each one. One core should exhibit low-loss guidance of the heating laser, i.e. low-loss guiding at the specific absorption wavelength of the gas, while the other core should exhibit low-loss guidance of the temperature probe pulse. Considering the wide transmission bands of many hollow-core fibers, it should be noted that a certain fiber element could be adapted to the detection of several types of molecules. This sensing structure, which in principle may seem complicated, could be developed either with a single engineered fiber (more complicated)

Optics EXPRESS

or, more likely, by developing a fiber bundle simply gluing two fibers with suitable characteristics. Since the two fibers have been proven already independently, there is no reason to believe that such an idea could not be developed.

However, one must keep in mind that a successful sensing fiber should also allow a convenient analyte flow into the structure at working pressure. For this purpose, there have already been some previous works with different proposals such as a *microchanneled* fiber [49–51], a *D-shaped* fiber [52, 53], exposed core fibers [1, 8], . . . The way of providing an access for the analyte to occupy the probed volume is indeed of key importance when designing a fast response detector. Depending on the fiber structure, the viscosity or capillary properties of the gas or fluid, the external pressure, etc., the time a surrounding fluid will take to replace the content of the fiber will range from minutes to hours [10, 54–57]. This is certainly a major point to address in the future.

6. Conclusions

In this paper, we have presented a proof-of-concept of a distributed optical fiber gas sensor based on thermal excitation of the target substance and its distributed temperature measurement through optical means. The method exploits the ability of a phase-sensitive ΦOTDR system to measure tiny (mK-range) temperature variations along a fiber optic line, while a pump laser is selectively heating the substance to be analyzed. This *photothermal distributed sensor* may show several advantages over other schemes devised up to now for distributed gas detection, among them: (i) specific coating elements on the fiber making the chemical transduction are no longer required; (ii) the possibility of developing the vast majority of the instrument at conventional telecom wavelengths and (iii) the possibility of distinguishing different substances by simply tuning the heating laser wavelength.

Further studies with other types of gas-filled fibers will be done in order to assess the full potential of this technique. Moreover, specific fiber designs could be of great interest, particularly those having different guiding mechanisms for the heating pump and the temperature probe pulse. Some details on these possible designs have also been discussed.

Funding

This work was supported in part by: the European Research Council through project U-FINE (Grant 307441); the EC Horizon 2020 program; the FINESSE project MSCA-ITN-ETN-722509; the DOMINO Water JPI project, under the WaterWorks2014 co-founded call by EC Horizon 2020 and Spanish MINECO; the Spanish MINECO (projects TEC2013-45265-R and TEC2015-71127-C2-2-R); and the regional program SINFOTON-CM: S2013/MIT-2790. The work of H. F. Martins was supported by EU funding (FP7 ITN ICONE program, gr. #608099). The work of Juan Pastor-Graells and S. Martín-López was supported by the Spanish MINECO (FPI and "Ramón y Cajal" contracts, respectively).